Quantification of normal cerebral oxygen extraction and oxygen metabolism by phase-based MRI susceptometry: evaluation of repeatability using two different imaging protocols.

Kämpe, Robin; Lind, Emelie; Ståhlberg, Freddy; van Westen, Danielle; Knutsson, Linda; Wirestam, Ronnie

Published in:
Clinical Physiology and Functional Imaging

DOI:
10.1111/cpf.12288

2017

Document Version:
Peer reviewed version (aka post-print)

Quantification of normal cerebral oxygen extraction and oxygen metabolism by phase-based MRI susceptometry: Evaluation of repeatability using two different imaging protocols

Robin Kämpe[1], Emelie Lind[1], Freddy Ståhlberg[1,2], Danielle van Westen[2,3], Linda Knutsson[1], Ronnie Wirestam[1]

1) Dept. of Medical Radiation Physics, Lund University, Sweden
2) Diagnostic Radiology, Department of Clinical Sciences, Lund, Lund University, Sweden
3) Imaging and Function, Skåne University Health Care, Lund, Sweden

Short title: Repeatability of normal OEF and $CMRO_2$ by MRI susceptometry

Received: 2 March 2015
Accepted 29 June 2015

Corresponding author:
Ronnie Wirestam
Dept. of Medical Radiation Physics
Lund University
University Hospital
SE-22185 Lund, Sweden
e-mail: ronnie.wirestam@med.lu.se

Abstract

Introduction: Global oxygen extraction fraction (OEF) and cerebral metabolic rate of oxygen ($CMRO_2$) were quantified in a test-retest study. Cerebral blood flow (CBF) data, required for $CMRO_2$ estimation, were obtained using dynamic susceptibility contrast MRI (DSC-MRI). OEF and $CMRO_2$ were quantified using two separate datasets, that is, conventional high-resolution (HR) gradient echo (GRE) phase maps as well as echo planar imaging (EPI) phase maps taken from the baseline (pre-contrast) part of the DSC-MRI time series. The EPI phase data were included to elucidate whether an extra HR-GRE scan is needed to obtain information about OEF and $CMRO_2$, or if this information can be extracted from the DSC-MRI experiment only. **Methods:** Twenty healthy volunteers were scanned using 3 T MRI on two occasions. Oxygen saturation levels were obtained from phase data measured in the great cerebral vein of Galen, based on HR-GRE as well as EPI phase maps. In combination with DSC-MRI CBF, this allowed for calculation of OEF and $CMRO_2$. **Results:** HR-GRE- and EPI-based phase images resulted in similar OEF spread and repeatability, with coefficients of variation/intra-class correlation coefficients of 0.26/0.95 and 0.23/0.81, respectively. Absolute OEF values (HR-GRE: 0.40±0.11, EPI: 0.35±0.08) were consistent with literature data. $CMRO_2$ showed similar repeatability, somewhat increased spread and reasonable absolute values (HR-GRE: 3.23±1.26 ml O_2/100g/min, EPI: 2.79±0.89 ml O_2/100g/min). **Discussion**: In general, the results obtained by HR-GRE and EPI showed comparable characteristics. The EPI methodology could potentially be improved by using a slightly modified DSC-MRI protocol (e.g., with regard to spatial resolution and slice gap).

Keywords: Magnetic resonance imaging, oxygen saturation, oxygen consumption, perfusion, brain

Introduction

During its passage through the microvasculature of the brain, oxygenated arterial blood is deoxygenated by release of a fraction of its oxygen molecules to the surrounding tissue. Deoxygenated blood is subsequently collected in major cerebral venous outflow vessels, for example, the internal jugular vein, the superior sagittal sinus and the great cerebral vein of Galen (below referred to as the vein of Galen) (Fernandez-Seara *et al.*, 2006; Jain *et al.*, 2010). Assessment of the oxygen saturation level of the blood in major cerebral veins enables estimation of the global oxygen delivery and cerebral oxygen consumption (Haacke *et al.*, 1997; Fernandez-Seara *et al.*, 2006; Donahue *et al.*, 2009). Knowledge of the blood oxygen saturation, either globally (by measuring in the major outflow veins) or locally (by measuring in other, smaller, veins), is important when it comes to understanding the physiology of the brain, evaluating oxygen supply in relevant diagnostic groups and assessing the overall vitality and function of the brain (Haacke *et al.*, 1997; Jain *et al.*, 2010; Sharf & El-Gebali, 2013). It has, for example, been shown that the jugular venous oxygen saturation correlates with the Glasgow coma scale (Sharf & El-Gebali, 2013). Furthermore, the oxygen extraction of the brain can be used to calculate the cerebral metabolic rate of oxygen ($CMRO_2$), which is of clinical and scientific relevance, for example, in differentiation between incipient and advanced late-onset Alzheimer's disease and in the understanding of the relationship between cerebral metabolism and the blood CO_2 level (connected with hypercapnia) (Siesjö, 1980; Hoyer *et al.*, 1991; Jain *et al.*, 2011; Xu *et al.*, 2011). Another example of clinical relevance is that a global measure of $CMRO_2$ could be used for treatment guidance in neonates with neonatal congenital heart disease, and thus reduce the risk of permanent brain damage (Jain *et al.*, 2014).

A common clinical approach to acquire a global measure of oxygen saturation is to acquire blood samples from the internal jugular vein bulb and then analyze them *in vitro,* or to continuously monitor the oxygen saturation using a fiber-optic catheter (van der Hoeven *et al.*, 1995; Trubiani *et al.*, 1996). Non-invasive methods are also available, for example, near infrared spectroscopy (NIRS)

for measurement of cortical and sub-cortical oxygenation in a region of the brain (Jöbsis, 1977; Colquhoun *et al.*, 2012), and positron emission tomography (PET) which has proven successful in regionally distinguishing viable from nonviable cerebral tissue (Powers *et al.*, 1985). Several magnetic resonance imaging (MRI) approaches have also been presented. For example, Wright *et al.* measured the oxygen saturation level in large blood vessels by *in vitro* calibration of the relationship between the oxygen saturation of the blood and the T2-value of blood, for conditions similar to the *in vivo* environment (Wright *et al.*, 2005). An & Lin proposed the use of blood oxygenation level-dependent contrast in combination with a signal model by Yablonskiy & Haacke (Yablonskiy & Haacke, 1994; An & Lin, 2000) for obtaining quantitative measures of cerebral blood oxygen extraction fraction. A more recent method for determining local oxygen saturation of venous blood was presented by Bolar *et al.,* based on velocity-selective spin labelling to isolate the MR signal originating from venous blood and subsequently determining its T2 for application of oxygen saturation calibration data (Bolar *et al.*, 2011). Xu et al. used phase-contrast MRI for quantitative global cerebral blood flow (CBF) measurement in combination with T2-relaxation-under-spin-tagging (TRUST) MRI for estimation of global $CMRO_2$ (Xu *et al.*, 2009).

In 1992, Weisskoff and Kiihne developed a technique to measure the absolute magnetic susceptibility by mapping the magnetic field perturbation using information from phase difference images (Weisskoff & Kiihne, 1992). In 2006, Fernández-Seara *et al.* presented a method (based on the phase approach by Weisskoff and Kiihne), which is very similar to the one used in the present work, to determine oxygen saturation in a major vein *in vivo* by MRI susceptometry (Fernandez-Seara *et al.*, 2006). The method requires no *in vitro* calibration, and is based on the relationship between oxygen saturation level and magnetic susceptibility. The basic methodology is to measure the phase of globally draining veins and their surrounding tissue in gradient echo (GRE) phase maps. The oxygen extraction fraction (OEF), closely related to the oxygen saturation, can then be calculated based on the fact that there is a difference in magnetic susceptibility between oxygenated and deoxygenated blood, extracted from the difference between the phase value of the venous blood and the phase

value of the surrounding tissue. Fan *et al.* combined MRI susceptometry and arterial spin labelling (ASL) CBF measurements for quantification of $CMRO_2$ in grey matter (Fan *et al.*, 2012).

The aim of the present study was to further evaluate MRI susceptometry, combined with CBF data, with regard to long-term repeatability (in 20 healthy volunteers) and MRI readout technique. The short-term repeatability (i.e., only a couple of minutes between measurements) has previously been investigated (Jain *et al.*, 2010), while we present a study design with at least one week between the scans. In addition, the method was applied not only to high-resolution (HR)-GRE phase images, but also to non-contrast-enhanced echo planar imaging (EPI) phase images from the baseline part of a DSC-MRI study. The EPI phase images were thus obtained as part of a regular DSC-MRI experiment, and did not require extra scan time. The venous oxygen saturation levels were converted to OEF, and the availability of global cerebral blood flow (CBF) information, from the DSC-MRI experiment, enabled additional calculation and analysis of $CMRO_2$ (under the assumption that oxygen saturation levels in the vein of Galen can represent global levels in normal subjects). Hence, we evaluated and compared OEF and $CMRO_2$ results extracted from both HR-GRE and EPI phase data in the same volunteers, at two different scanning sessions.

Theory

The difference in magnetic susceptibility between oxyhemoglobin and de-oxyhemoglobin leads to differences between the phase shifts of the MRI signals in arterial and venous blood. Assuming that arterial blood is fully oxygenated, the measured difference in phase between venous blood and the surrounding tissue is converted to magnetic susceptibility and this provides the blood oxygen saturation, which in turn can be translated into information about the uptake or extraction of oxygen in the brain.

The phase difference $\Delta\Phi$ between venous blood and surrounding tissue is given by:

$$\Delta\Phi = \gamma \cdot \Delta B \cdot TE, \tag{1}$$

where ΔB is the difference in local magnetic field between the vein and the surrounding tissue, γ is the gyromagnetic constant and TE is the echo time. The difference in local magnetic field will depend on the oxygen saturation level of the venous blood and the orientation of the vein relative the static external magnetic field. Assuming an infinitely long cylindrical vessel, the difference in magnetic field is given by:

$$\Delta B = \frac{\Delta\chi}{6} \cdot (3\cos^2\Theta - 1) \cdot B_0, \tag{2}$$

where $\Delta\chi$ is the difference in magnetic susceptibility between the venous blood and the surrounding tissue and Θ is the angle between the vessel and the external magnetic field B_0. The difference in magnetic susceptibility is related to the oxygen saturation level of the venous blood and the hematocrit (Hct) level (assuming an arterial oxygen saturation of 100 %):

$$\Delta\chi = \Delta\chi_{do} \cdot Hct \cdot (1 - Y_v), \tag{3}$$

where $\Delta\chi_{do} = 4\pi \cdot 0.18$ ppm per unit Hct is the difference in blood magnetic susceptibility between deoxygenated and oxygenated blood (Haacke *et al.*, 1999), and Y_v is the venous oxygen saturation level. According to Eqs 1-3, the relationship between measured phase difference and venous oxygen saturation level is given by:

$$Y_v = 1 - \frac{6 \cdot \Delta\Phi}{\gamma \cdot \Delta\chi_{do} \cdot (3\cos^2\Theta - 1) \cdot Hct \cdot B_0 \cdot TE} \quad (4)$$

The oxygen extraction fraction (OEF) is defined as:

$$OEF = 1 - Y_v\,. \quad (5)$$

The OEF can, in combination with the corresponding CBF data, be used to calculate the cerebral metabolic rate of oxygen ($CMRO_2$). Again, assuming the arterial oxygen saturation to be equal to 100 %, the $CMRO_2$ is given by:

$$CMRO_2 = OEF \cdot CBF \cdot C_a = OEF \cdot CBF \cdot MCHC \cdot Hct \cdot c \quad (6)$$

C_a = [Hb]·c = MCHC·Hct·c is the oxygen concentration of the blood, where [Hb] is the concentration of hemoglobin in the blood, *c* is the Hb-carrying capacity of oxygen and MCHC is the mean corpuscular Hb concentration in red blood cells. In the present study, we used Hct=0.4 (Guyton & Hall, 2000a), MCHC=34 g/dl (Guyton & Hall, 2000b), and c=$1.368\ \mathrm{ml/g}$ (Dijkhuizen *et al.*, 1977).

Methods

Subjects and MRI experiments

All experiments were performed on a 3 T MRI scanner with an 8-channel head coil (Philips Healthcare, Best, The Netherlands). A total of 20 healthy volunteers (10 males, 10 females, age 25-84 years) were included in the study, after participation in a neurological physical examination, including basic cognitive testing. Each subject was examined on two occasions (test-retest), separated by 7-20 days. The study was approved by the local ethics committee, and written informed consent was obtained from each volunteer. Calculations of $CMRO_2$ in the present study required knowledge of CBF results collected in connection with a previous study (Knutsson *et al.*, 2014), and this is indicated by appropriate citations below.

For high-resolution phase mapping, 3D double-echo GRE images with flow compensation were acquired using TEs of 20 ms and 40 ms. Magnitude as well as phase images were collected for 50 axial slices orthogonal to the external magnetic field, with spatial resolution $0.98 \cdot 0.98 \cdot 1.15\ \mathrm{mm}^3$, field of view (FOV) = $220 \cdot 220\ \mathrm{mm}^2$, repetition time (TR) = 45 ms, flip angle (FA) = 20°, bandwidth = 218 Hz/pixel.

For EPI phase mapping (using the DSC-MRI protocol further described below), 2D single echo images with flow compensation were acquired using a TE of 29 ms. Magnitude and phase images were collected for 20 axial slices, with spatial resolution $1.72 \cdot 1.72 \cdot 5\ \mathrm{mm}^3$, FOV = $220 \cdot 220\ \mathrm{mm}^2$, FA = 60 °, SENSE factor = 2.5, bandwidth = 1256 Hz/pixel.

Perfusion measurements for global CBF quantification were carried out using the DSC-MRI protocol: Single-shot GRE EPI at a temporal resolution of 1.24 s. Contrast agent (0.1 mmol/kg, Dotarem, Guerbet, Paris, France) was injected at an injection rate of 5 mL/s followed by a saline flush. In the DSC-MRI experiment, *Smart-Exam* (Young *et al.*, 2006) was used for planning of the slice orientation.

A pre-bolus administration approach for AIF rescaling was also carried out prior to the conventional DSC-MRI experiment (Knutsson *et al.*, 2014). A pre-bolus dose of contrast agent (0.02 mmol/kg b.w) was injected at a rate of 5 mL/s. Segmented EPI was used to track the pre-bolus passage through the sagittal sinus in one single slice, at a temporal resolution of 0.81 s, in order to acquire a venous output function (VOF). The imaging parameters of the pre-bolus experiment were FOV 220×220 mm^2, image matrix 128×128, slice thickness 5 mm, EPI factor 7, flip angle 22°, TR 135 ms, TE 15 ms, SENSE factor 2.2.

MRI data post-processing

Estimates of CBF were calculated according to Eq. 7:

$$CBF = \frac{(1 - H_{large})R_{max} \int_0^\infty C_t(t)dt}{\rho(1 - H_{small}) \int_0^\infty R(t)dt \cdot 5 \int_0^\infty VOF(t)dt} \quad (7)$$

where the tissue impulse response function R(t) was obtained by block-circulant singular value decomposition deconvolution of measured tissue concentration time curves $C_t(t)$ with an AIF, and R_{max} is the peak value of R(t). VOF(t) is the first-pass venous concentration curve from the pre-bolus experiment, H_{large} and H_{small} are the haematocrit values in large and small vessels, respectively, and ρ is the whole-brain mass density, and the numerical value of $(1\text{-}H_{large})/[\ \rho\ (1\text{-}H_{small})]$ was set to 0.705 cm^3/g. A global AIF, used in the deconvolution, was obtained from middle cerebral artery branches in the Sylvian fissure region. CBF was calculated pixel by pixel, and a global mean CBF value was extracted for calculation of global $CMRO_2$. Further details of CBF data acquisition and calculation are given by Knutsson et al. (2014).

The HR-GRE phase images with TE=40 ms suffered from severe aliasing effects (which the unwrapping algorithm failed to resolve) near large vessels, and were not suitable for further analysis, leaving only phase images with TE=20 ms (HR-GRE phase images) and TE=29 ms (EPI phase images). These phase images were unwrapped using a region-growing algorithm (Cusack & Papadakis, 2002),

and subsequently filtered to remove background gradients, using the "projection onto dipole fields (PDF)" method (Liu *et al.*, 2011).

ROIs were drawn by hand in both the vein of Galen and in tissue surrounding the vessel (Figure 1). The ROIs included, for the HR-GRE phase images, 1-9 voxels in the vein of Galen and about 120-170 voxels in the background tissue. Due to slice gaps and lower spatial resolution in EPI, the ROIs in the EPI phase images typically included 1-3 voxels in the vein of Galen and about 24-45 voxels in the background tissue. To compensate for the small number of voxels in the EPI vessel ROIs, the ROI was applied to as many of the EPI volumes in the time series as possible (varying from 3 to 13), and a mean phase value over the different time points was extracted.

The angle of the vein of Galen relative the external magnetic field was determined by visual inspection of the HR-GRE image volume (where slices were orthogonal to the main magnetic field) using image-viewing software (ImageJ, 1.47v, Wayne Rasband, National Institutes of Health, USA) (Figure 2). The extracted phase values and the vessel angle were then used to calculate OEF according to Eqs 4-5. The OEF estimates were, in combination with CBF (Eq. 7), subsequently used for calculation of $CMRO_2$ according to Eq. 6.

Statistics

Repeatability was assessed by comparing visit 1 with visit 2 using the intra-class correlation coefficient (ICC) (Two-Way Mixed Model, Consistency, Single Measure). The spread was evaluated by the coefficient of variation (CV). Bland-Altman plots (Bland & Altman, 1986) were used to compare pairs of resulting datasets (i.e., test versus retest and HR-GRE versus EPI). For the HR-GRE versus EPI Bland-Altman analyses, standard deviations were compensated for repeated measurements in each subject (denoted SD_C). In order to further analyze the HR-GRE versus EPI groups, linear correlation analyses of Bland-Altman data as well as t-tests of mean values (two tailed, two sampled, paired) were performed.

Results

The angle between the vein of Galen and the external magnetic field could, for each volunteer, be approximated to 0° in the OEF calculations. The results from the *in vivo* measurements of OEF and $CMRO_2$ are summarized in Table 1.

HR-GRE phase data as well as EPI phase data provided good OEF repeatability, with ICCs above 0.8, as seen in Table 1 (ICCs of 0.95 and 0.81, respectively). The OEF variability between volunteers, however, was somewhat large for both datasets, as can be seen in Table 1 (CVs of 0.26 and 0.23, for HR-GRE and EPI, respectively). These results imply a slightly larger spread between volunteers in the HR-GRE phase data, and in Fig. 3 a larger range of OEF values can be seen for HR-GRE. Similar conclusions can be drawn regarding the $CMRO_2$ repeatability, as both HR-GRE and EPI provided high ICCs (0.90 and 0.84, respectively). The $CMRO_2$ spread between volunteers was, however, heavily increased compared to the OEF spread as can be seen in Table 1 (CVs of 0.40 and 0.33, for HR-GRE and EPI, respectively). In the calculation of $CMRO_2$, the same CBF values were used for both HR-GRE and EPI, so the increases in $CMRO_2$ variability were about the same for both methods, and more or less the same relationship between the two datasets is maintained as for OEF, i.e., a slightly larger spread between volunteers for HR-GRE (*cf.* Figure 4).

The t-tests showed that the HR-GRE population mean values of both OEF and $CMRO_2$ were significantly higher ($p < 0.05$) than the corresponding OEF and $CMRO_2$ estimates extracted from EPI data. The OEF Bland-Altman plot (Figure 5b) clearly visualizes one apparent outlier (>2SD), while most of the OEF and $CMRO_2$ data points show reasonably small differences between HR-GRE and EPI. However, linear regression analysis of the $CMRO_2$ Bland-Altman data indicated a correlation coefficient of 0.5 ($p<0.05$), potentially indicating the presence of a systematic effect or proportional error.

Discussion

The test-retest measure ICC was high (>0.8) for both datasets, for OEF as well as $CMRO_2$, which is encouraging considering that several days passed between the imaging sessions. A time span of several days implies slight differences in position as well as fluctuations in overall physiology and cerebral activity of the volunteers between the different scanning occasions. Hence, the method seems to be consistent on an individual level, for both HR-GRE and EPI phase data. Jain *et al.* investigated the short-term repeatability of a very similar methodology and observed a slightly higher repeatability (ICC = 0.94) for $CMRO_2$ measurements in the superior sagittal sinus (Jain *et al.*, 2010). These volunteers were instructed to rise and reposition between scans (a total of three scans were preformed) and to stay alert during the scans. It is reasonable to assume that the short time between measurements in the study by Jain et al. explains the slightly higher repeatability compared with the present study.

OEF and $CMRO_2$ show a natural biological variation between subjects (Hattori *et al.*, 2004; Lu & Ge, 2008; Jain *et al.*, 2010; Seubert & Mahla, 2014), related to, for example, differences in age and minor fluctuations associated with current state of stress and cerebral activity. It is still fair, however, to conclude that the investigated MRI method returned an inter-individual OEF variation that was slightly high, for both datasets. This excessive inter-individual spread may partly originate from the fact that measurements had to be conducted with slight differences in geometry and vessel availability between volunteers. The exact choice of voxels to be included in the vessel ROI had considerable impact on the resulting phase, probably due to partial volume effects, and this problem mainly affected measurements in volunteers where the vessel showed limited visibility. Due to the low spatial resolution of EPI data, the vessel was often subjectively more difficult to locate in the EPI images but this did not seem to cause any additional variability. Part of the variability was most likely caused by differences in the anatomy of the volunteers. For example, the infinitely long cylinder approximation might not be appropriate for all volunteers. According to Beuf *et al.*, the ratio of the

vessel length to the vessel diameter should be above 4 (Beuf *et al.*, 1996), and this ratio for the vein of Galen was estimated to be between 2 and 4 in the present material. Additionally, beyond the straight segment, the vessel bends and, for some volunteers, it can run relatively close to the straight segment and this might affect the measured phase. One potential solution to avoid these issues would be to try to find other vessel candidates for phase measurements. One obvious candidate is the superior sagittal sinus, which is often regarded to be the standard location, but this vessel is located very close to the interface between soft tissue and bone, which could affect the phase value and create aliasing issues. Another vessel candidate is the internal jugular vein, but phase images of this vessel are known to suffer from severe susceptibility artifacts because the vessel runs close to the air-filled oral cavity and trachea (Jain *et al.*, 2010). Considering the problems associated with other major veins, in combination with the fact that it was indeed possible to identify a large and fairly straight vessel segment of the vein of Galen in all volunteers, the vein of Galen can still be regarded as a good choice, in spite of the geometry issues, although care must be taken to optimize the imaging conditions. Furthermore, although the superior sagittal sinus is more of a standard choice, the direct comparison between HR-GRE and EPI is still relevant since the same vessel was used for both methods.

The CV for $CMRO_2$ was increased compared with OEF. It is not unrealistic for $CMRO_2$ to show large variability in viable brain tissue, when subjects over a large age interval are studied (Powers *et al.*, 1985). However, a large part of the increased variability can most likely be attributed to the fact that the prebolus-calibrated DSC-MRI CBF data, used to calculate $CMRO_2$ from OEF, also shows substantial inherent variability. The pre-bolus version of DSC-MRI, employed in the present study, is expected to perform better than standard DSC-MRI implementations for quantitation of CBF in absolute terms (Knutsson *et al.*, 2010), but uncertainties related to, for example, manual VOF registration, remaining arterial partial volume effects (affecting the AIF shape), competing T1-weighting effects, T2* relaxivity issues and a potentially non-linear relationship between $\Delta R2^*$ and concentration in whole blood are likely to remain (Knutsson *et al.*, 2014).

Another potential reason for the observed OEF and $CMRO_2$ variability is that constant literature values of Hct, MCHC and c (*cf.* Eqs. 4 and 6), related to oxygen content of arterial blood, were employed in this study. Although fixed values have been applied also in similar previous studies of OEF determination (e.g., Haacke *et al.*, 1997; Jain *et al.*, 2010), we acknowledge that actual hematocrit/hemoglobin levels, and thus the oxygen contents, differ between men and women and that inter-subject variations may be considerable. However, our assessment of repeatability as well as comparisons between HR-GRE and EPI, which are the primary scopes of this study, should not be substantially influenced by individual variations in Hct and oxygen content. The variability was, in overall terms, very similar between the two datasets (i.e., HR-GRE vs. EPI), although the CV was slightly higher for HR-GRE, for both OEF and $CMRO_2$. This small difference might be explained by differences in signal to noise ratio (SNR) and/or partial volume effects between the HR-GRE and EPI datasets.

With regard to absolute levels, the OEF population means extracted from HR-GRE phase data and EPI phase data were both in reasonable agreement with the literature. According to standard text books (Patel *et al.*, 2014) the normal OEF is 0.30-0.45, and studies using MRI (Lu & Ge, 2008; Jain *et al.*, 2010) and PET (Hattori *et al.*, 2004) have reported OEF mean values in the range 0.36-0.39. Hattori et al. reported the full range (min-max) of observed OEF values to be 0.30-0.51. The resulting $CMRO_2$ mean values were also in agreement with the literature, where text books (Seubert & Mahla, 2014) indicate 3.0-3.5 ml O_2/100g/min (or 125-146 µmol O_2/100g/min) as the normal $CMRO_2$ level, and MRI (Xu *et al.*, 2009; Jain *et al.*, 2010) and PET (Hattori *et al.*, 2004) methods have resulted in mean values ranging from 2.85 to 3.17 ml O_2/100g/min (or 119-132 µmol O_2/100g/min). In the study by Hattori et al., the full range (min-max) of observed $CMRO_2$ values was 2.35-3.84 ml O_2/100g/min.

Even though HR-GRE phase data and EPI phase data provided OEF and $CMRO_2$ mean values in general agreement with the literature, it should still be noted that HR-GRE returned significantly higher values than EPI. When observing the Bland-Altman plots (Figures 5b and 6b), one can see that

the results are in reasonable to good agreement between the two datasets, except for a few data points, where HR-GRE phase data showed unexpectedly high values. The overall slightly lower EPI results (compared with HR-GRE) could potentially be explained by more pronounced EPI partial volume effects and a correspondingly lower average phase value in the voxels of the blood vessel. It is difficult, however, to determine the relevance of this effect since both HR-GRE phase data and EPI phase data produced OEF and $CMRO_2$ values in agreement with the literature. The potential issues with the EPI data could be reduced by minor alterations to the EPI scanning protocol, for example, by slightly increasing the spatial resolution to avoid partial volume effects and by eliminating slice gaps, provided, of course, that acceptable SNR and brain coverage can be maintained. As pointed out above, spread and repeatability, for both OEF and $CMRO_2$, were about the same for HR-GRE and EPI results. This implies that, from these aspects, one would not gain much by performing extra HR-GRE scans after the DSC-MRI protocol. The main discrepancy between HR-GRE and EPI in the obtained results is the significant difference in mean values of both OEF and $CMRO_2$.

It is worth noting that only one TE was available for each dataset (20 ms for HR-GRE and 29 ms for EPI), i.e., no subtraction between phase maps with different TEs was performed. Others have used two phase maps with shorter TEs and subsequently used the difference between the two, to avoid phase bias and aliasing issues (Fernandez-Seara *et al.*, 2006; Shmueli *et al.*, 2009; Jain *et al.*, 2010). A phase bias may thus potentially have existed in our phase maps (e.g., arising due to local differences in conductivity), but it has been argued that the effect of this bias is negligible (Haacke *et al.*, 1997; Haacke *et al.*, 1999). Furthermore, the employed TEs were slightly long, leading to some minor aliasing issues that, for some volunteers, caused an unclear vessel structure in the images which made it difficult to find an appropriate location for the measurements (also causing extra variability between volunteers). To address this problem, and thus increase the accuracy of the estimates, the acquisition protocol could be optimized with regard to vessel imaging, for example, by acquiring several phase images with additional TEs, which would allow for better unwrapping and bias reduction. For the EPI acquisition, this could possibly be obtained by using a double echo in the EPI

sequence, to avoid the need for extra scans. If only one or two TEs are to be used, they should be short, due to the aliasing mentioned above. Another source of error is the ROI positioning and the limited ROI size in vessels. Obviously, the ROIs were selected to be as large as possible, but were constrained by the size and visibility of the vessel. This problem would also be reduced by the improvements suggested above.

In conclusion, both HR-GRE and EPI phase data resulted in absolute global OEF and $CMRO_2$ mean values which were consistent with literature data. EPI-based phase acquisition, within a conventional DSC-MRI protocol, worked reasonably well for quantitative global OEF and $CMRO_2$ assessment and showed generally good correspondence with HR-GRE results (Figs. 5-6) This implies that an extra HR-GRE scan is redundant, alternatively that additional global OEF and $CMRO_2$ data can be obtained from an already existing DSC-MRI perfusion measurement (provided that phase maps are made available from the DSC-MRI experiment).

Acknowledgements

This study was supported by the Swedish Research Council (grants no. 13514, 2007–3974, 2010-4454 and 2011-2971), and the Swedish Cancer Society (grant no. 2012/597).

Conflict of Interest

The authors have no conflicts of interest.

References

An H, Lin W. Quantitative measurements of cerebral blood oxygen saturation using magnetic resonance imaging. *J Cereb Blood Flow Metab* (2000); **20**: 1225-1236.

Beuf O, Briguet M, Lissac M, Davis R. Magnetic resonance imaging for the determination of magnetic susceptibility of materials. *J Magn Reson* (1996); **112**: 111-118.

Bland JM, Altman DG. Statistical methods for assessing agreement between two methods of clinical measurement. *Lancet* (1986); **327**: 307-310.

Bolar DS, Rosen BR, Sorensen AG, Adalsteinsson E. QUantitative Imaging of eXtraction of Oxygen and TIssue Consumption (QUIXOTIC) using venular-targeted velocity-selective spin labeling. *Magn Reson Med* (2011); **66**: 1550-1562.

Colquhoun DA, Tucker-Schwartz JM, Durieux ME, Thiele RH. Non-invasive estimation of jugular venous oxygen saturation: A comparison between near infrared spectroscopy and transcutaneous venous oximetry. *J Clin Monit Comput* (2012); **26**: 91-98.

Cusack R, Papadakis N. New robust 3-D phase unwrapping algorithms: application to magnetic field mapping and undistorting echoplanar images. *Neuroimage* (2002); **16**: 754-764.

Dijkhuizen P, Buursma A, Fongers TME, Gerding AM, Oesburg B, Zijlstra WG. The oxygen binding capacity of human haemoglobin. *Pflugers Arch* (1977); **369**: 223-231.

Donahue MJ, Blicher JU, Ostergaard L, Feinberg DA, Macintosh BJ, Miller KL, Gunther M, Jezzard P. Cerebral blood flow, blood volume, and oxygen metabolism dynamics in human visual and motor cortex as measured by whole-brain multi-modal magnetic resonance imaging. *J Cereb Blood Flow Metab* (2009); **29**: 1856-1866.

Fan AP, Benner T, Bolar DS, Rosen BR, Adalsteinsson E. Phase-based regional oxygen metabolism (PROM) using MRI. *Magn Reson Med* (2012); **67**: 669-678.

Fernandez-Seara MA, Techawiboonwong A, Detre JA, Wehrli FW. MR susceptometry for measuring global brain oxygen extraction. *Magn Reson Med* (2006); **55**: 967-973.

Guyton AC, Hall JE, The body fluid compartments: Extracellular and intracellular fluids; interstitial fluid and edema. In: *Textbook of Medical Physiology* (2000a); pp. 290-306. Saunders, Philadelphia.

Guyton AC, Hall JE, Red blood cells, anemia, and polycythemia. In: *Textbook of Medical Physiology* (2000b); pp. 419-428. Saunders, Philadelphia.

Haacke M, Lai S, Reichenbach JR, Kuppusamy K, Hoogenraad FGC, Takeichi H, Lin W. In vivo measurement of blood oxygen saturation using magnetic resonance imaging: A direct validation of the blood oxygen level-dependent concept in functional brain imaging. *Hum Brain Mapp* (1997); **5**: 341-346.

Haacke M, Brown R, Thompson M, Venkatesan R, Magnetic properties of tissues: Theory and measurement. In: *Magnetic Resonance Imaging: Physical Principles and Sequence Design* (1999); pp. 741-779. Wiley-Liss, New York.

Hattori N, Bergsneider M, Wu HM, Glenn TC, Vespa PM, Hovda DA, Phelps ME, Huang SC. Accuracy of a method using short inhalation of ^{15}O-O_2 for measuring cerebral oxygen extraction fraction with PET in healthy humans. *J Nucl Med* (2004); **45**: 765-770.

Hoyer S, Nitsch R, Oesterreich K. Predominant abnormality in cerebral glucose utilization in late-onset dementia of the Alzheimer type: a cross-sectional comparison against advanced late-onset and incipient early-onset cases. *J Neural Transm* (1991); **3**: 1-14.

Jain V, Langham MC, Wehrli FW. MRI estimation of global brain oxygen consumption rate. *J Cereb Blood Flow Metab* (2010); **30**: 1598-1607.

Jain V, Langham MC, Floyd TF, Jain G, Magland JF, Wehrli FW. Rapid magnetic resonance measurement of global cerebral metabolic rate of oxygen consumption in humans during rest and hypercapnia. *J Cereb Blood Flow Metab* (2011); **31**: 1504-1512.

Jain V, Buckley EM, Licht DJ, Lynch JM, Schwab PJ, Naim MY, Lavin NA, Nicolson SC, Montenegro LM, Yodh AG, Wehrli FW. Cerebral oxygen metabolism in neonates with congenital heart disease quantified by MRI and optics. *J Cereb Blood Flow Metab* (2014); **34**: 380-388.

Jöbsis FF. Non-invasive infrared monitoring of cerebral and myocardial oxygen sufficiency and circulatory parameters. *Science* (1977); **198**: 1264-1267.

Knutsson L, Ståhlberg F, Wirestam R. Absolute quantification of perfusion

using dynamic susceptibility contrast MRI: pitfalls and possibilities. *Magn Reson Mater Phy* (2010); **23**: 1-21.

Knutsson L, Lindgren E, Ahlgren A, Van Osch MJ, Markenroth Bloch K, Surova Y, Ståhlberg F, Van Westen D, Wirestam R. Dynamic susceptibility contrast MRI with a prebolus contrast agent administration design for improved absolute quantification of perfusion. *Magn Reson Med* (2014); **72**: 996-1006.

Liu T, Khalidov I, De Rochefort L, Spincemaille P, Liu J, Tsiouris AJ, Wang Y. A novel background field removal method for MRI using projection onto dipole fields (PDF). *NMR Biomed* (2011); **24**: 1129-1136.

Lu H, Ge Y. Quantitative evaluation of oxygenation in venous vessels using T2-relaxation-under-spin-tagging MRI. *Magn Reson Med* (2008); **60**: 357-363.

Patel PM, Drummond JC, Lemkuil BP, Cerebral physiology and the effects of anesthetic drugs. In: *Miller's Anesthesia* (ed. Miller, R.D.) (2014); vol. 1, pp. 387-423. Elsevier, Amsterdam.

Powers WJ, Grubb RL Jr, Darriet D, Raichle ME. Cerebral blood flow and cerebral metabolic rate of oxygen requirements for cerebral function and viability in humans. *J Cereb Blood Flow Metab* (1985); **5**: 600-608.

Seubert CN, Mahla ME, Neurologic monitoring. In: *Miller's Anesthesia* (ed. Miller, R.D.) (2014); vol. 1, pp. 1487-1524. Elsevier, Amsterdam.

Sharf MS, El-Gebali MA. Correlation between Glasgow coma scale and jugular venous oxygen saturation in severe traumatic brain injury. *Egypt J Anaesth* (2013); **29**: 267-272.

Shmueli K, De Zwart JA, Van Gelderen P, Li TQ, Dodd SJ, Duyn JH. Magnetic susceptibility mapping of brain tissue in vivo using MRI phase data. *Magn Reson Med* (2009); **62**: 1510-1522.

Siesjö BK. Cerebral metabolic rate in hypercarbia - A controversy. *J Anaesthesiol* (1980); **52**: 461-465.

Trubiano P, Heyer EJ, Adams DC, Mcmahon DJ, Christiansen I, Rose EA, Delphin E. Jugular venous bulb oxyhemoglobin saturation during cardiac surgery: Accuracy and reliability using a continuous monitor. *Anesth Analg* (1996); **82**: 964-968.

Van Der Hoeven JG, de Koning J, Compier EA, et al. Early jugular bulb oxygenation monitoring in comatose patients after an out-of-hospital cardiac arrest. *Intensive Care Med* (1995); **21**: 567-572.

Weisskoff RM, Kiihne S. MRI susceptometry: Image-based measurement of absolute susceptibility of MR contrast agents and human blood. *Magn Reson Med* (1992); **24**: 375-383.

Wright GA, Hu BS, Macovski A. Estimating oxygen saturation of blood in vivo with MR imaging at 1.5 T. *J Magn Reson Imaging* (1991); **1**: 275-283.

Xu F, Ge Y, Lu H. Noninvasive quantification of whole-brain cerebral metabolic

rate of oxygen ($CMRO_2$) by MRI. *Magn Reson Med* (2009); **62**: 141-148.

Xu F, Uh J, Brier MR, Hart JJ, Yezhuvath US, Gu H, Yang Y, Lu H. The influence of carbon dioxide on brain activity and metabolism in conscious humans. *J Cereb Blood Flow Metab* (2011); **31**: 58-67.

Yablonskiy DA, Haacke M. Theory of NMR signal behavior in magnetically inhomogeneous tissues: The static dephasing regime. *Magn Reson Med* (1994); **32**: 749-763.

Young S, Bystrov D, Netsch T, Bergmans R, Van Muiswinkel A, Visser F, Sprigorum R, Gieseke J. Automated planning of MRI neuro scans. *Proc SPIE* (2006); **6144**: 61441M.

Table 1

Population mean value, SD, CV and ICC for OEF and $CMRO_2$ results from HR-GRE as well as EPI. SD and CV are based on mean values of results from visit 1 and visit 2. The required CBF estimates from Knutsson et al. (2014) are also provided for completeness.

	Method	Mean±SD	CV	ICC
OEF	HR-GRE	0.40 ± 0.11 %	0.26	0.95
	EPI	0.35 ± 0.08 %	0.23	0.81
$CMRO_2$	HR-GRE	134 ± 53 μmol O_2/100g/min 3.23 ± 1.26 ml O_2/100g/min	0.39	0.90
	EPI	116 ± 37 μmol O_2/100g/min 2.79 ± 0.89 ml O_2/100g/min	0.32	0.84
Global mean CBF	Pre-bolus DSC-MRI (Knutsson *et al.*, 2014)	43.6 ± 14.6 ml/100g/min		

Figure captions

Figure 1.

Illustration of the placement of a typical (a) background ROI (in blue) and (b) vessel ROI (in green) in the HR-GRE phase images. In (b), a zoomed-in view of the red square in (a) is shown. The corresponding ROIs for the EPI data are shown in (c) and (d). Note that white/black represents a phase value of ±1.5 radians or more in (a) and (c), while white/black corresponds to a phase value of ±3.0 radians or more in (b) and (d).

Figure 2.

Illustration of how the angle between the vessel and the external magnetic field was determined. By observing the vein of Galen in three different orientations, the angle could be assessed.

Figure 3.

OEF test-retest scatter plots (solid line is line of identity) and Bland-Altman plots calculated from (a, b) HR-GRE phase data and (c, d) EPI phase data.

Figure 4.

$CMRO_2$ test-retest scatter plots (solid line is line of identity) and Bland-Altman plots calculated from (a, b) HR-GRE phase data and (c, d) EPI phase data.

Figure 5.

(a) The mean OEF value of visit 1 and visit 2 calculated from EPI phase data plotted against the corresponding value calculated from HR-GRE phase data. The blue line is the line of identity. (b) The x-axis of the Bland-Altman plot illustrates the OEF spread amongst the volunteers. The y-axis shows the OEF difference between HR-GRE and EPI phase data. Linear correlation analysis of the displayed Bland-Altman data indicated that the correlation coefficient r was not significantly different from zero ($p>0.05$).

Figure 6.

(a) The mean $CMRO_2$ value of visit 1 and visit 2 calculated from EPI phase data plotted against the corresponding value calculated from HR-GRE phase data. The blue line is the line of identity. (b) The x-axis of the Bland-Altman plot illustrates the $CMRO_2$ spread amongst the volunteers. The y-axis shows the $CMRO_2$ difference between HR-GRE and EPI phase data. Linear correlation analysis of the displayed Bland-Altman data resulted in $r= 0.50$ ($p=0.025$).

Figure 1

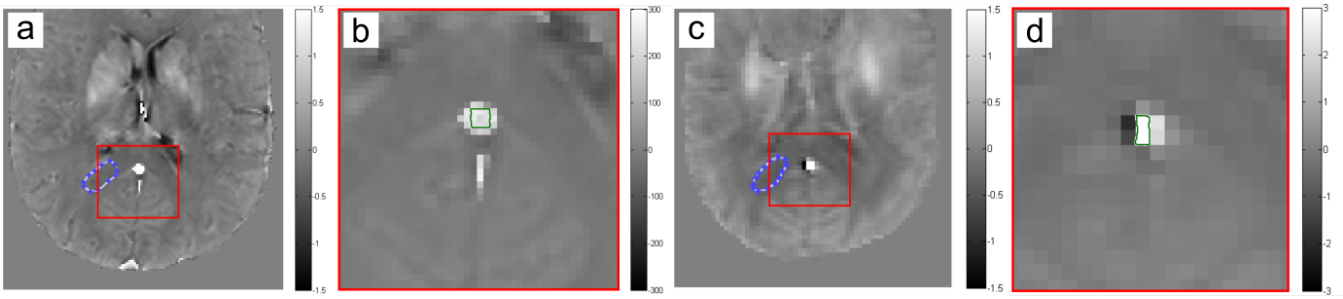

Figure 2

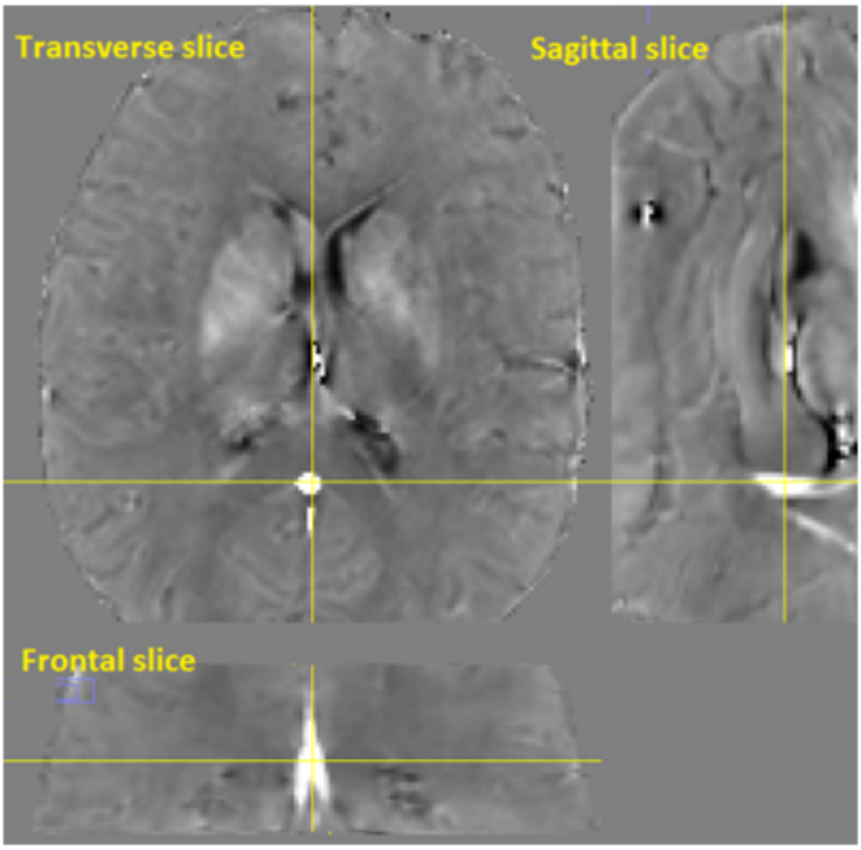

Figure 3

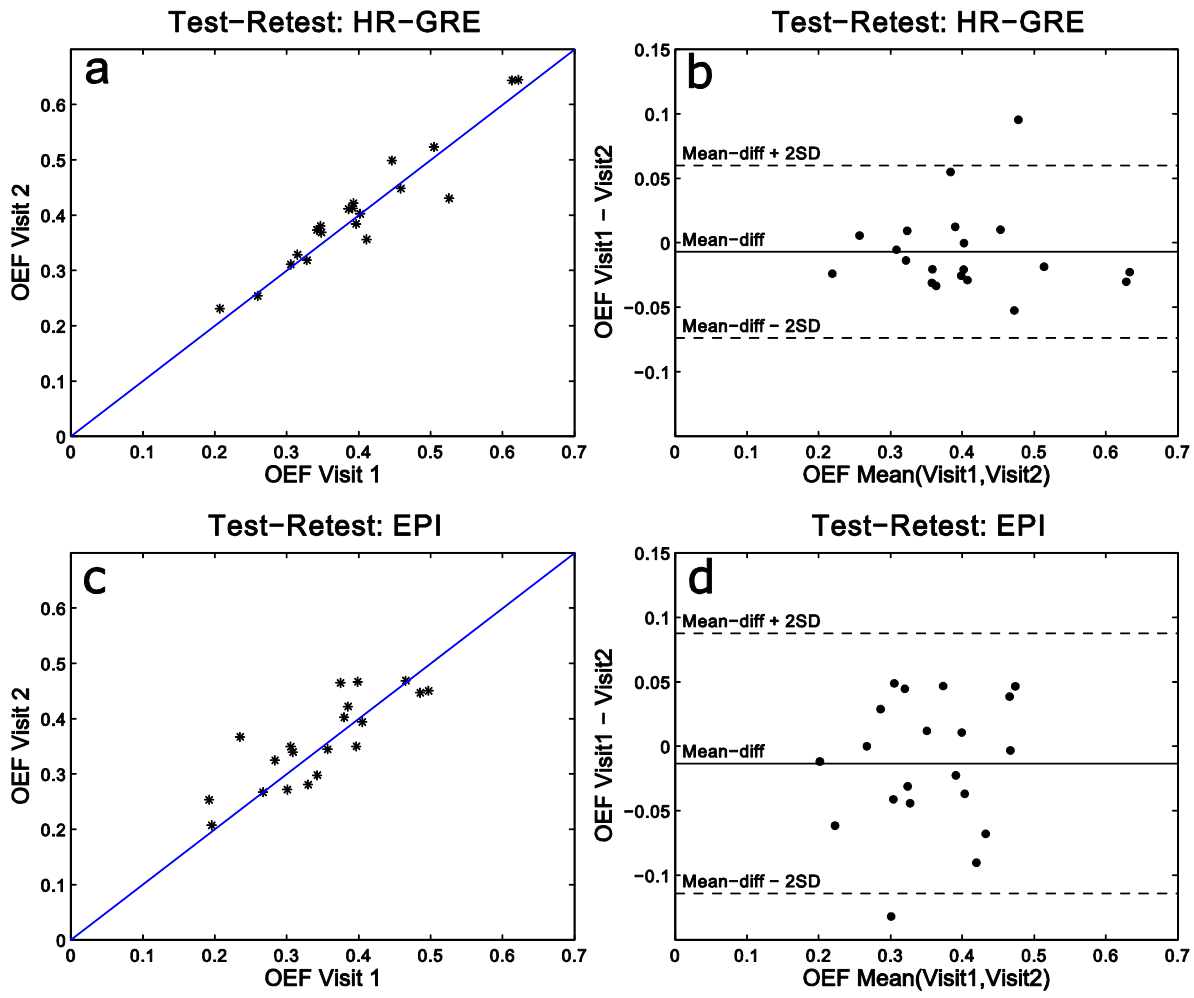
Test−Retest: HR−GRE
a
OEF Visit 2
OEF Visit 1
Test−Retest: HR−GRE
b
Mean−diff + 2SD
Mean−diff
Mean−diff − 2SD
OEF Visit1 − Visit2
OEF Mean(Visit1,Visit2)
Test−Retest: EPI
c
OEF Visit 2
OEF Visit 1
Test−Retest: EPI
d
Mean−diff + 2SD
Mean−diff
Mean−diff − 2SD
OEF Visit1 − Visit2
OEF Mean(Visit1,Visit2)

Figure 4

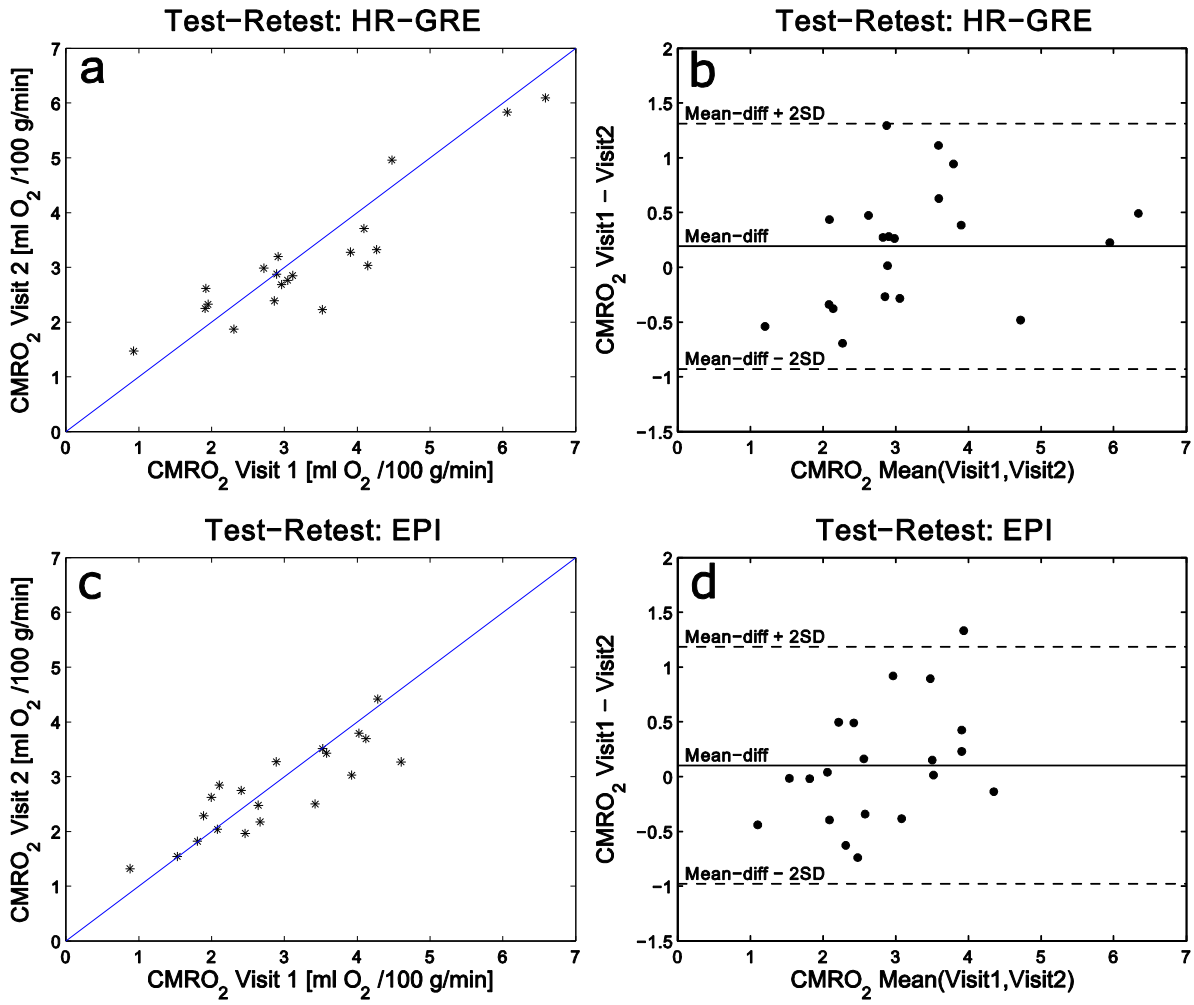
Test−Retest: HR−GRE
a
CMRO2 Visit 2 [ml O2 /100 g/min]
CMRO2 Visit 1 [ml O2 /100 g/min]
Test−Retest: HR−GRE
b
Mean−diff + 2SD
Mean−diff
Mean−diff − 2SD
CMRO2 Visit1 − Visit2
CMRO2 Mean(Visit1,Visit2)
Test−Retest: EPI
c
CMRO2 Visit 2 [ml O2 /100 g/min]
CMRO2 Visit 1 [ml O2 /100 g/min]
Test−Retest: EPI
d
Mean−diff + 2SD
Mean−diff
Mean−diff − 2SD
CMRO2 Visit1 − Visit2
CMRO2 Mean(Visit1,Visit2)

Figure 5

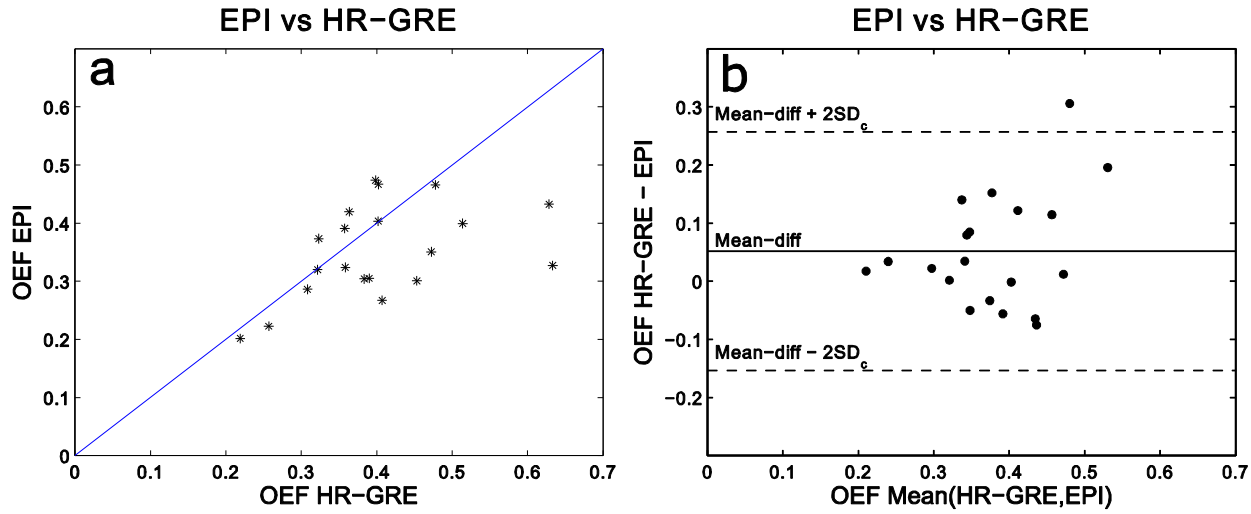
EPI vs HR−GRE
a
OEF EPI
OEF HR−GRE
0
0.1
0.2
0.3
0.4
0.5
0.6
0.7
EPI vs HR−GRE
b
Mean−diff + 2SDc
Mean−diff
Mean−diff − 2SDc
OEF HR−GRE − EPI
OEF Mean(HR−GRE,EPI)
−0.2
−0.1
0
0.1
0.2
0.3

Figure 6

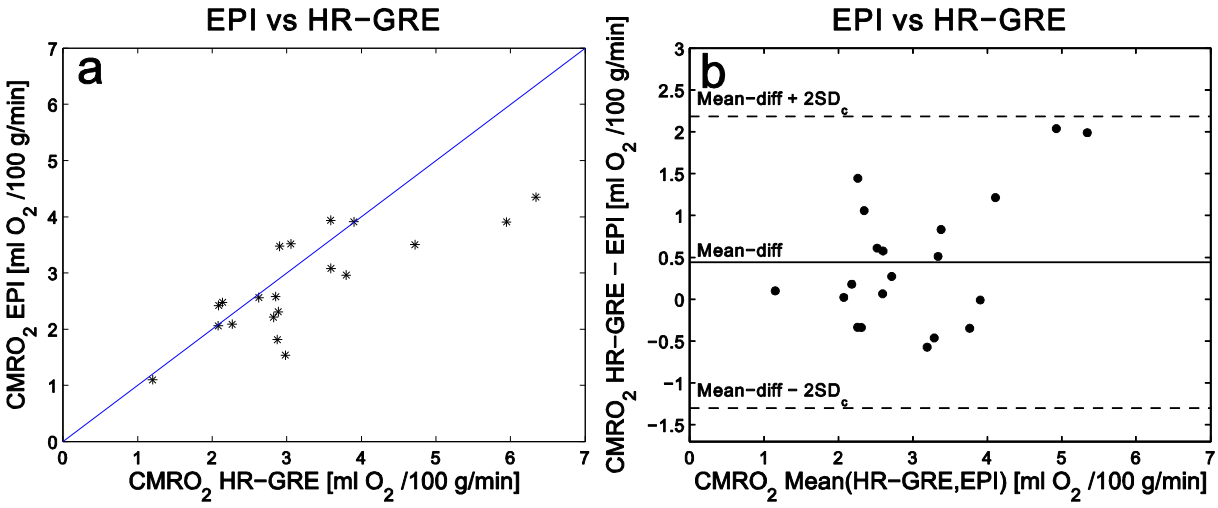
EPI vs HR−GRE
a
CMRO2 EPI [ml O2 /100 g/min]
CMRO2 HR−GRE [ml O2 /100 g/min]
EPI vs HR−GRE
b
Mean−diff + 2SDc
Mean−diff
Mean−diff − 2SDc
CMRO2 HR−GRE − EPI [ml O2 /100 g/min]
CMRO2 Mean(HR−GRE,EPI) [ml O2 /100 g/min]